Supplementary Material

High performance $LiMn_{0.8}Fe_{0.2}PO_4$@C cathode material constructed by a novel intermediate hydrated $MnHPO_4$ for lithium-ion batteries

Taotao Zeng[a,b], Dai-Huo Liu[b,c], Changling Fan*[,a,d], Runzheng Fan[a], Fuquan Zhang[a,d], Jinshui Liu*[,a,d], Tingzhou Yang[b], Zhongwei Chen*[,b]

[a] *College of Materials Science and Engineering, Hunan University, Changsha 410082, China.*

[b] *Department of Chemical Engineering, Waterloo Institute for Nanotechnology, Waterloo Institute for Sustainable Energy, University of Waterloo, Waterloo, Ontario N2L 3G1, Canada.*

[c] *Collaborative Innovation Center of Henan Province for Green Manufacturing of Fine Chemicals, Key Laboratory of Green Chemical Media and Reactions, Ministry of Education, School of Chemistry and Chemical Engineering, Henan Normal University, Xinxiang, 453007, China.*

[d] *Hunan Province Key Laboratory for Advanced Carbon Materials and Applied Technology, Hunan University, Changsha 410082, China.*

* Corresponding author. Tel.: +1 519-888-4567 ext. 38664; fax: +86 731 88822967.

E-mail address: fancl@hnu.edu.cn (Dr. C.-L. Fan);
jshliu@hnu.edu.cn (Prof. J.-S. Liu);
zhwchen@uwaterloo.ca (Prof. Z.-W. Chen).

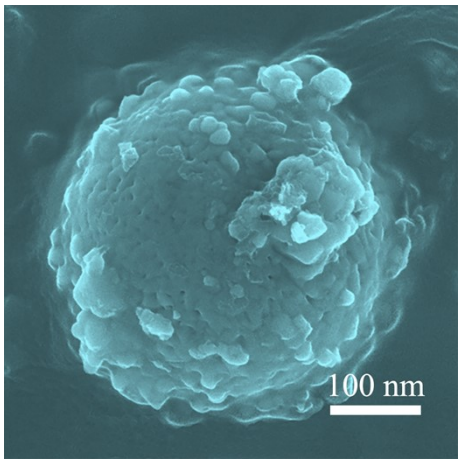

Fig. S1 SEM image of LMFP-0.5 (×60,000).

During the sintering process, $LiMn_{0.8}Fe_{0.2}PO_4$ nanoparticles were formed and the grains covered with a uniform pyrolytic carbon bubble-layer. Fig. S1 shows SEM image of the morphology of nanoparticle under the magnification of ×60,000. The size of nanoparticle is about 250 nm with spherical-like shape.

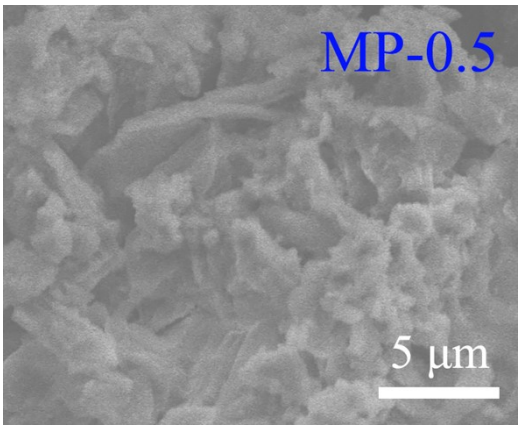

Fig. S2 SEM image of MP-0.5

The morphology of unsintered sample MP-0.5 is shown in Fig. S2. It can be seen that the unsintered particles are irregular in shape with obvious agglomeration of hydrated $MnHPO_4$. Therefore, the high-energy ball milling method can be used to refine the crystal grain size and improve the agglomeration.

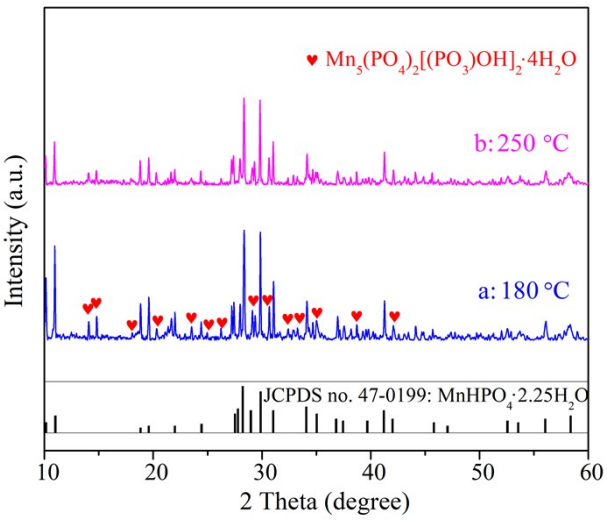

Fig. S3 XRD pattern of MP-0.5 (sintered at 180 and 250 °C for 2 h)

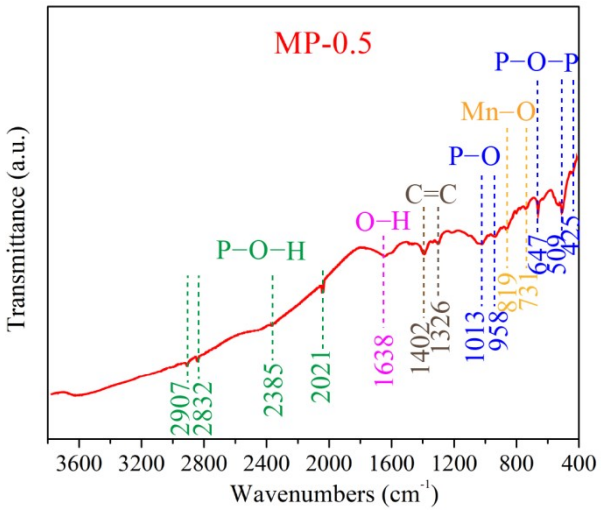

Fig. S4 FT-IR spectra of MP-0.5

According to FT-IR spectra of $MnHPO_4 \cdot 2.25H_2O$ (Fig. S4), the vibrational bands of HPO_4^{2-} are located at 2907, 2832, 2385 and 2021 cm^{-1} are assigned to the asymmetric stretching of $\nu_{OH}(HPO_4^{2-})$ and symmetric stretching of $\nu_{OH}(HPO_4^{2-})$, respectively.[1,2] The band of 1638 cm^{-1} is attributed to O–H bending mode of H_2O molecule of crystalline hydrate.[1] The bands of 1402 and 1326 cm^{-1} are assigned to stretching vibration of C=C.[3] The bands at 819 and 731 cm^{-1} are the main attributed to the stretching vibration of Mn–O groups.[4] The bands of 1100 - 900 and 650 - 500 cm^{-1} are mainly attributed to the intramolecular vibrations of PO_4^{3-}. The strong bands around 958 and 1013 cm^{-1} are assigned to symmetric stretching $\nu_1(A_1)$ and asymmetric stretching $\nu_3(F_2)$ modes of P–O, respectively. Meanwhile, the bands at around 627 and 509 cm^{-1} are attributed to the resolved triply $\nu_4(F_2)$ and doubly $\nu_2(E)$ degenerate bending and stretching modes of P–O–P, respectively. The FT-IR spectra of $MnHPO_4 \cdot 2.25H_2O$ is similar to that of $MgHPO_4 \cdot 3H_2O$ measured by Boonchom et al.[5]

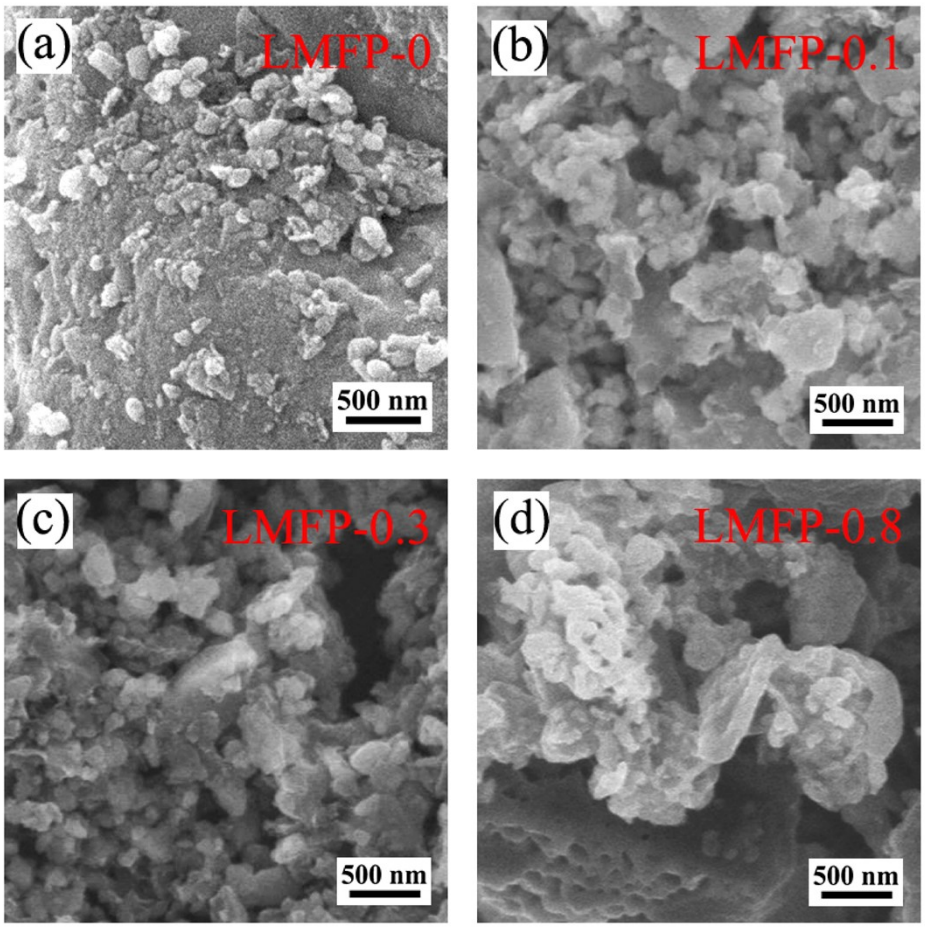

Fig. S5 SEM images of (a) LMFP-0, (b) LMFP-0.1, (c) LMFP-0.3 and (d) LMFP-0.8.

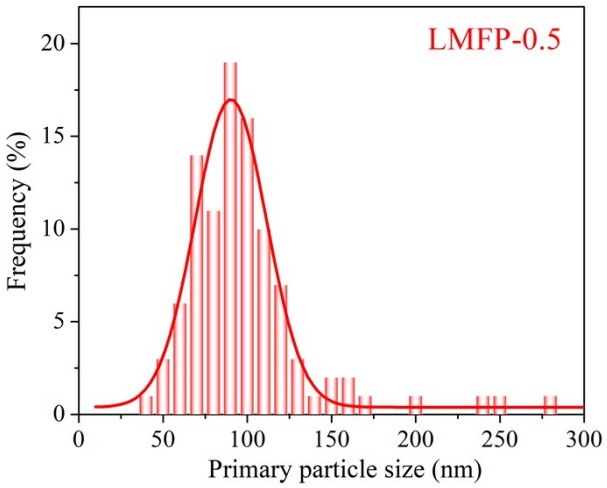

Fig. S6 Primary particle size distribution of LMFP-0.5

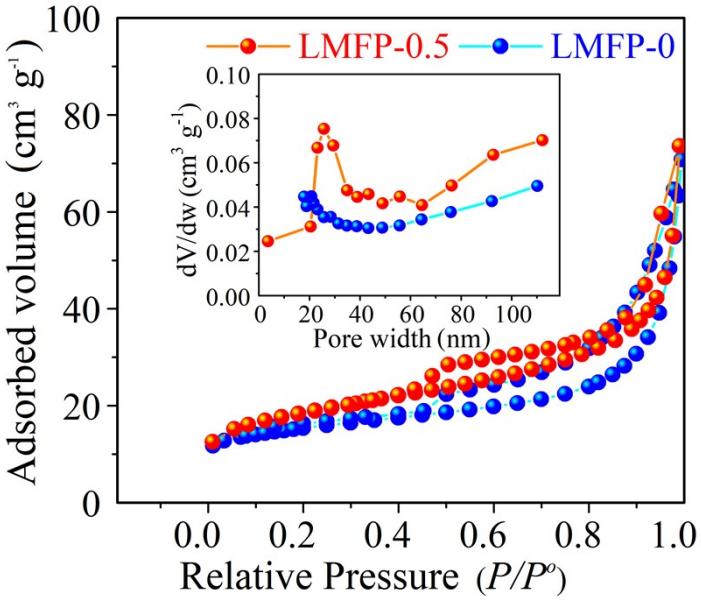

Fig. S7 Nitrogen adsorption-desorption isotherms and pore size distribution (inset) of LMFP-0.5 and LMFP-0.

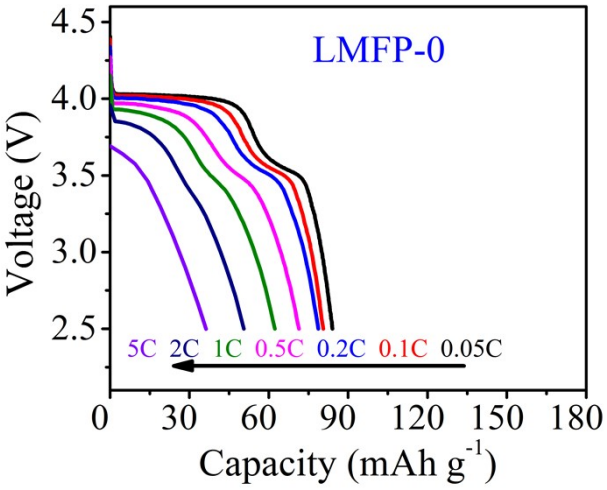

Fig. S8 Discharge profiles at different rates of LMFP-0.

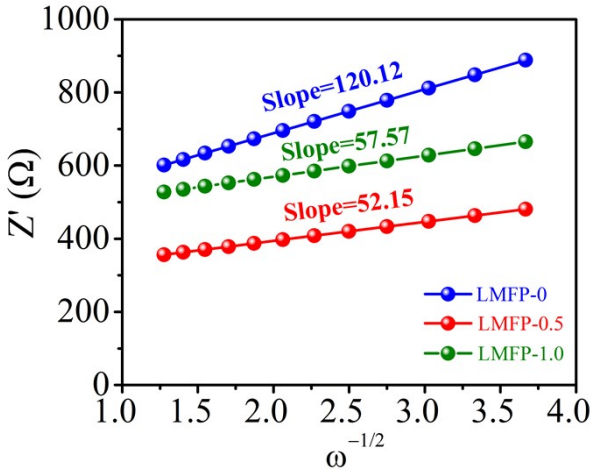

Fig. S9 The relationship between Z' and $\omega^{-1/2}$ at the low-frequency region for samples.

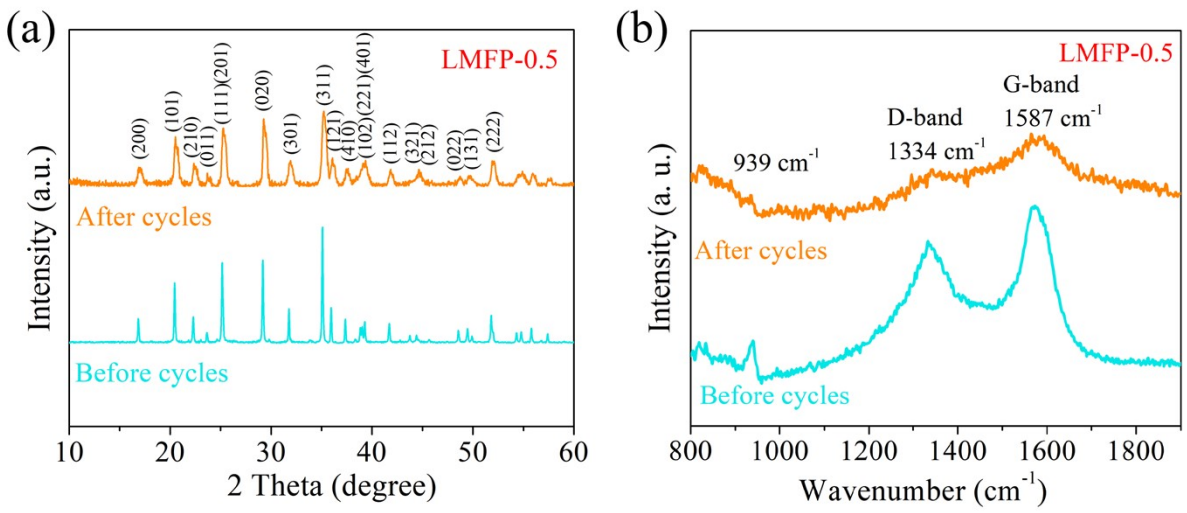

Fig. S10 Ex-situ (a) XRD and (b) Raman patterns of cathode films of LMFP-0.5 before and after 200 cycles.

Table S1 Lattice parameters and cell volume of samples

Samples	*a*/Å	*b*/Å	*c*/Å	*V*/Å^3
LMFP-0	10.431	6.089	4.738	300.92
LMFP-0.1	10.435	6.095	4.730	300.52
LMFP-0.3	10.433	6.087	4.741	300.75
LMFP-0.5	10.439	6.090	4.736	300.98
LMFP-0.8	10.440	6.091	4.743	300.19
LMFP-1.0	10.441	6.083	4.738	301.47

Table S2 Mass content, molar and molar ratio of elements in LMFP-0.5

Elements	Li	Mn	Fe	P
mass content / %	2.563	15.717	3.791	10.996
Molar / mol	0.369	0.286	0.068	0.355
molar ratio	1.040	0.806	0.191	1.000

Table S3 Redox peak interval $\triangle V_1$(Mn) and $\triangle V_2$(Fe), charge-transfer resistance (R_{ct}), exchange current density (i_0) and Li^+ diffusion coefficient (D_{Li+}) of samples

Samples	**$\triangle V_1$(Mn)**	**$\triangle V_2$(Fe)**	**R_{ct}/Ω**	**i_0/mA cm^{-2}**	**D_{Li}^+/cm^2 s^{-1}**
LMFP-0	0.52	0.27	396.9	0.065	2.084×10^{-15}
LMFP-0.5	0.37	0.18	201.3	0.128	1.106×10^{-14}
LMFP-1.0	0.49	0.26	340.7	0.075	9.072×10^{-15}

Table S4 Comparisons of the precursors, synthetic strategies and performances between this work and the previously reported $LiMn_{0.8}Fe_{0.2}PO_4$@C cathode materials.

Materials	Precursor	Method for precursor	Primary particle size (nm)	Capacity (mA h g^{-1})	Cyclic performance	Ref.
$LiMn_{0.8}Fe_{0.2}PO_4$@C	$MnHPO_4·2.25H_2O$ FeC_2O_4	Sol-gel reaction and ball-milling	50~100	153.9 (0.05 C) 130.1 (1 C) 75.9 (5 C)	95.84% (100 cycles@0.05 C) 98.62% (100 cycles@1 C)	**This work**
$LiMn_{0.8}Fe_{0.2}PO_4$-C	$MnPO_4·H_2O$ FeC_2O_4	Ball-milling	200~300	99.5 (0.1 C) 78.3 (0.5 C)	92% (50 cycles@0.5 C)	6.
$LiMn_{0.8}Fe_{0.2}PO_4$	$Mn_{0.8}Fe_{0.2}PO_4$	Solid-state reaction	80	148 (0.1 C)	/	7.
$LiMn_{0.8}Fe_{0.2}PO_4$/C	$Mn_{0.8}Fe_{0.2}C_2O_4·2H_2O$	Solid-state reaction and ball-milling	100~150	142.7 (0.1 C) 129.8 (1 C) 112.6 (5 C)	95.4% (300 cycles@1 C)	8.
$LiMn_{0.8}Fe_{0.2}PO_4$/C	$Mn_3(PO_4)_2·3H_2O$ FeC_2O_4	Ball-milling	50	159 (0.1 C) 148 (1 C) 138 (5 C)	95% (500 cycles@1 C) 92% (500 cycles@5 C)	9.
$LiMn_{0.8}Fe_{0.2}PO_4$/C	$Mn_{0.8}Fe_{0.2}PO_4·2H_2O$	Co-precipitation method	30~50	151.1 (0.1 C) 129.8 (1 C) 98.4 (5 C) 82 (10 C)	/	10.
$LiMn_{0.8}Fe_{0.2}PO_4$/C	$(Mn_{0.8}Fe_{0.2})_3(PO_4)_2·xH_2O$	Co-precipitation method	100	150.0 (0.05 C) 130.0 (1 C) 110.3 (5 C)	95.1% (300 cycles@1 C)	11.

References

1. C. Sronsri, P. Noisong and C. Danvirutai, Solid state reaction mechanisms of the $LiMnPO_4$ formation using special function and thermodynamic studies, *Ind. Eng. Chem. Res.*, 2015, **28**, 7083-7093.
2. J. Chen, X. Lan, C. Wang and Q. Zhang, The formation mechanism and corrosion resistance of a composite phosphate conversion film on AM60 alloy, *Mater. (Basel)*, 2018, **11**, 1996.
3. H. Wang, X. Zhang, F. Zheng, Y. Huang and Q. Li, Surfactant effect on synthesis of core-shell $LiFePO_4$/C cathode materials for lithium-ion batteries, *J. Solid State*

Electrochem., 2015, **19**, 187.

4. G. Qiu, Z. Gao, H. Yin, X. Feng, W. Tan and F. Liu, Synthesis of $MnPO_4 \cdot H_2O$ by refluxing process at atmospheric pressure, *Solid State Sci.,* 2010, **12**, 808.
5. B. Boonchom, Kinetic and thermodynamic studies of $MgHPO_4 \cdot 3H2O$ by non-isothermal decomposition data, *J. Therm. Anal. Calorim.,* 2009, **98**, 863.
6. T. Liu, B. Wu and X. Wu, Realizing Fe substitution through diffusion in preparing $LiMn_{1-x}Fe_xPO_4$-C cathode materials from $MnPO_4 \cdot H_2O$, *Solid State Ionics*, 2014, **254**, 72-77.
7. Y. Mishima, C. Moriyoshi and Y. Kuroiwa, Electrochemical and structural study on $LiMn_{0.8}Fe_{0.2}PO_4$ and $Mn_{0.8}Fe_{0.2}PO_4$ battery cathodes: diffusion limited lithium transport, *J. Solid State Electr.*, 2017, **21**, 3221-3228.
8. G. Hu, Y. Wang, K. Du, Z. Peng, X. Xie and Y. Cao, Synthesis and characterization of $LiMn_{0.8}Fe_{0.2}PO_4$/rGO/C for lithium-ion batteries via in-situ coating of $Mn_{0.8}Fe_{0.2}C_2O_4 \cdot 2H_2O$ precursor with graphene oxide, *J. Solid State Electr.*, 2020, **24**, 2441-2450.
9. Z. Peng, B. Zhang, G. Hu, K. Du, X. Xie, K. Wu, J. Wu, Y. Gong, Y. Shu and Y. Cao, Green and efficient synthesis of micro-nano $LiMn_{0.8}Fe_{0.2}PO_4$/C composite with high-rate performance for Li-ion battery, *Electrochim. Acta*, 2021, **387**, 138456.
10. K. Du, L.H. Zhang, Y.B. Cao, Z.D. Peng and G.R. Hu, Synthesis of $LiMn_{0.8}Fe_{0.2}PO_4$/C by co-precipitation method and its electrochemical performances as a cathode material for lithium-ion batteries, *Mater. Chem. Phys.*, 2012, **136**, 925-929.
11. Y. Wang, G. Hu, Y. Cao, Z. Peng, X. Lai, X. Xie and K. Du, Highly atom-economical and environmentally friendly synthesis of $LiMn_{0.8}Fe_{0.2}PO_4$/rGO/C cathode material for lithium-ion batteries, *Electrochim. Acta*, 2020, **354**, 136743.